



ON THE FORMATION OF AMIDE POLYMERS VIA CARBONYL–AMINO GROUP LINKAGES IN ENERGETICALLY PROCESSED ICES OF ASTROPHYSICAL RELEVANCE

MARKO FÖRSTEL^{1,2}, PAVLO MAKSYUTENKO^{1,2}, BRANT M. JONES^{1,2}, BING J. SUN³,
HUAN C. LEE³, AGNES H. H. CHANG³, AND RALF I. KAISER^{1,2}

¹Department of Chemistry, University of Hawaii, 2545 McCarthy Mall, 96822 HI, USA; ralfk@hawaii.edu

²W. M. Keck Research Laboratory in Astrochemistry, University of Hawaii, 2545 McCarthy Mall, 96822 HI, USA

³Department of Chemistry, National Dong Hwa University, Shoufeng, Hualien 974, Taiwan; hhchang@mail.ndhu.edu.tw

Received 2015 November 3; accepted 2016 February 10; published 2016 March 29

ABSTRACT

We report on the formation of organic amide polymers via carbonyl–amino group linkages in carbon monoxide and ammonia bearing energetically processed ices of astrophysical relevance. The first group comprises molecules with one carboxyl group and an increasing number of amine moieties starting with formamide (45 u), urea (60 u), and hydrazine carboxamide (75 u). The second group consists of species with two carboxyl (58 u) and up to three amine groups (73 u, 88 u, and 103 u). The formation and polymerization of these linkages from simple inorganic molecules via formamide and urea toward amide polymers is discussed in an astrophysical and astrobiological context. Our results show that long chain molecules, which are closely related to polypeptides, easily form by energetically processing simple, inorganic ices at very low temperatures and can be released into the gas phase by sublimation of the ices in star-forming regions. Our experimental results were obtained by employing reflectron time-of-flight mass spectroscopy, coupled with soft, single photon vacuum ultraviolet photoionization; they are complemented by theoretical calculations.

Key words: astrobiology – astrochemistry – ISM: molecules – methods: laboratory: molecular – molecular processes

Supporting material: machine-readable tables

1. INTRODUCTION

During the last decade, the astrochemical origin of the peptide bond (–CO–NH–) in extraterrestrial environments has received considerable attention both from the astronomy and astrobiology communities (Ehrenfreund 1999; Ehrenfreund & Charnley 2000; Peeters et al. 2003). The formamide molecule (HCONH₂) as detected in the interstellar medium (ISM; Gottlieb et al. 1973; Hollis et al. 2006; Halfen et al. 2011; Adande et al. 2013) represents the simplest molecule carrying the amide (peptide) bond (Figure 1). Very recently, Jones et al. (2011) elucidated the formation mechanism of formamide in astrophysically relevant ices exposed to energetic electrons via the radical–radical recombination of formyl (HCO) with the amidogen radical (NH₂) inside astrophysically relevant ices at 10 K. The next homologue molecule in this series—urea (CO(NH₂)₂)—was also detected in processed ices online and in situ, exploiting photoionization of the subliming molecules during the temperature programmed desorption (TPD) phase via tunable vacuum ultraviolet (VUV) light and by detecting the parent ion through a reflectron time-of-flight mass spectrometer (PI-ReTOF-MS; Förstel et al. 2015a). It is also well established that amino acids (Bernstein et al. 2002; Muñoz Caro et al. 2002; Elsila et al. 2007; Chen et al. 2008; Hudson et al. 2008) and their formal condensation products—dipeptides—as complex as Glycylglycine (Gly-Gly) and Leucyl-Alanine (Leu-Ala) can be synthesized abiotically in energetically processed ices (Kaiser et al. 2013; Figure 1). Note that formamide (HCONH₂) might act as a key intermediate in the synthesis of amino acids (Dederichs et al. 1975; Apene & Mikstais 1978; Kostakis et al. 2007). Further condensation reactions, possibly with the help of mineral catalysts such as olivine can then lead to the formation of even more complex

molecules like polypeptides (Costanzo et al. 2007; Saladino et al. 2007, 2013; Lambert 2008; Lambert et al. 2009). For clarification, we note that the –CO–NH– bond, often called a “peptide bond,” is strictly an amide bond unless the carbon and nitrogen are bonded to other carbons of amino acids. While a polypeptide contains amide bonds that are synonymously called peptide bonds, a polyamide with amide bonds is not a polypeptide.

Considering the identification of biorelevant molecules, formamide (HCONH₂) was first detected toward Sgr A and Sgr B2 by Gottlieb et al. (1973) and subsequently confirmed by Hollis et al. (2006), Halfen et al. (2011), and Adande et al. (2013). Halfen et al. determined fractional abundances in the range from 5.3×10^{-11} to 1.3×10^{-10} . The methyl-substituted analog—acetamide (CH₃CONH₂)—was observed toward Sgr B2(N) with fractional abundances of 2×10^{-11} to 2×10^{-10} (Hollis et al. 2006; Halfen et al. 2011); a tentative detection of urea (CO(NH₂)₂) was reported by Remijan et al. (2014) toward Sgr B2(N-LMH). Also, the very first mass spectra measured on a comet (67P/Churyumov Gerasimenko) revealed four new complex organic molecules (COM)—two of them (formamide and acetamide) carrying the peptide bond (Goesmann et al. 2015). Additionally, more than 80 amino acids were identified in meteorites such as Murcheson and the Lonewolf Nunataks 94102 (Kvenvolden et al. 1970; Cronin & Chang 1993; Glavin et al. 2006; Elsila et al. 2007). A detailed isotopic analysis (D/H; ¹³C/¹²C, ¹⁵N/¹⁴N) provided compelling evidence that these molecules were formed in the ISM (Robert & Epstein 1982; Yang & Epstein 1983; Cronin & Chang 1993; Alexander et al. 1998). However, with the exception of formamide (HCONH₂; Jones et al. 2011), the underlying formation mechanisms of the COM carrying the peptide bond are far from being understood.

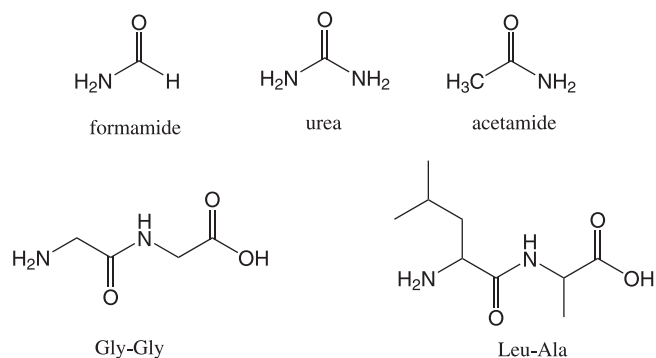


Figure 1. Peptide bond carrying molecules that were identified in energetically processed ices of astrophysical relevance.

Here we show that molecules that carry one or more peptide bonds can be easily synthesized abiotically via non-thermal (non-equilibrium) chemistry when simple astrophysical model ices consisting of ammonia (NH₃) and carbon monoxide (CO) are exposed to ionizing radiation in form of energetic electrons at ultralow temperatures as low as 5 K. These energetic electrons are generated within the track of energetic galactic cosmic rays (GCRs) penetrating the ice-coated nanoparticles (interstellar grains) in cold molecular clouds (Johnson 1990; Bennett et al. 2004, 2005). The detection of these molecules is made possible by exploiting a newly commissioned space simulation chamber and detecting the subliming molecules online and in situ in the gas phase. This approach utilizes tunable, soft VUV photoionization coupled with a reflectron time-of-flight mass spectrometer (PI-ReTOF-MS), and allows for a virtually fragmentation-free detection of subliming molecules in the TPD phase with superior sensitivity compared to conventional mass spectroscopy utilizing electron impact ionization.

2. EXPERIMENTAL AND THEORETICAL METHODS

2.1. Experimental

Our experiments were performed at the W.M. Keck Research Laboratory in Astrochemistry (Jones & Kaiser 2013; Jones et al. 2014; Kaiser et al. 2014b; Maity et al. 2014b) exploiting a next generation surface scattering machine. A gaseous mixture of ammonia (NH₃, 99.99% Matheson TriGas) and carbon monoxide (CO, 99.9% Matheson TriGas) with a ratio of 8 to 5 at 260 Torr was deposited onto a 5.5 ± 0.1 K silver target using a glass capillary array. The deposition was monitored using helium–neon (He–Ne) laser interferometry to determine the thickness of the ice (Hudgins et al. 1993; Westley et al. 1998; Fulvio et al. 2009). With a refractive index of the mixed ice of 1.3 ± 0.1 determined via the method outlined by Baratta & Palumbo (1998), Romanescu et al. (2010), and Satorre et al. (2013), we calculate the thickness of the deposited ice to be 500 ± 50 nm. The ratio of ammonia (NH₃) to carbon monoxide (CO) after the deposition was determined to be 4 ± 1 to 1, as calculated via infrared spectroscopy using known column densities as derived from the integrated absorption coefficients of the infrared absorption features of ammonia and carbon monoxide: the CO ν_1 band at 2139 cm^{-1} with $1.1 \times 10^{-17} \text{ cm mol}^{-1}$ (Gerakines et al. 1995) and the NH₃ ν_2 band at 1092 cm^{-1} with $1.7 \times 10^{-17} \text{ cm mol}^{-1}$ (d’Hendecourt & Allamandola 1986).

After the deposition, the ice was irradiated with mono-energetic electrons with kinetic energies of 5 keV impinging on the ice surface at an angle of 70° . The irradiation current was set to 15 nA to avoid secondary collisions with processed molecules. The irradiation time was one hour. The resulting dose per irradiated molecule was determined with the help of the Monte Carlo simulations (CASINO; Drouin et al. 2007) and established to be $2.2 \pm 0.2 \text{ eV}$ per NH₃ molecule and $1.1 \pm 0.2 \text{ eV}$ per CO molecule (Appendix; Table 2). Before, during, and after the irradiation, the FTIR spectra of the ices were recorded in a range of $600\text{--}6000 \text{ cm}^{-1}$, with a resolution of 4 cm^{-1} (FTIR, Nicolet 6700) online and in situ. One hour after the irradiation, the irradiated ices were warmed up at a constant rate of 0.5 K min^{-1} to 300 K. The subliming molecules were probed using soft VUV photoionization coupled with a reflectron time-of-flight mass spectrometer (PI-ReTOF-MS; Jones & Kaiser 2013). Two experiments were conducted with distinct ionization energies of 10.49 and 9.0 eV. Briefly, 10.49 eV photons were generated by frequency tripling of the third harmonic of an Nd:YAG (354.7 nm; Spectra Physics, PRO-250, 30 Hz) laser in a jet of pulsed xenon (Xe) gas (Maity et al. 2014a, 2014b). The 9.0 eV photons were produced using resonant four-wave mixing of two frequencies ($\omega_1; \omega_2$) in a pulsed xenon (Xe) gas (Hilbig & Wallenstein 1982; Hilbig et al. 1986; Hepburn 1994). The first beam was generated using the frequency doubled output of a dye laser (Syrah, Cobra-Stretch), which was pumped by the third harmonic of an Nd:YAG laser. In detail, the 354.6 nm output of the Nd:YAG was coupled with the dye laser containing a 0.25 g l^{-1} Coumarin440 (Exciton) in an ethanol (Pharmco Aaper, ACS/USP grade) solution. The resulting 445.12 nm light was then doubled using a BBO (Sirah, 57°4) crystal to yield 222.56 nm light. The second laser beam was generated using the direct output of a dye laser (Sirah, Precision Scan) filled with a 0.16 g l^{-1} Pyrromethene557 (Exciton) dissolved in ethanol. This dye laser was pumped with the second harmonic of an Nd:YAG laser (532 nm) producing light with a wavelength of 579 nm. Both laser beams were then coupled using a dichroic mirror (CVI Melles Griot, LWP-45-RP222-TP633-PW-1025-UV) and led into a differentially pumped vacuum chamber through a magnesium fluoride (MgF₂) window. A fused silica biconvex lens (Thorlabs LB4265, $f = 150 \text{ mm}$) focused both beams into a section of a pulsed jet of xenon released by a piezoelectric pulsed valve operated at 30 Hz. A lithium fluoride (LiF) lens mounted off-center from the beam path of the generated and fundamental laser beams spatially separated the beams according to their refractive indices. A pin hole behind this lens was then used to block the fundamentals ($\omega_1; \omega_2$) from entering the interaction region, and only the 9.0 eV light was introduced into the main chamber. The intensity of the laser beams was monitored using a copper Faraday cup mounted behind the interaction region, based on the photoelectric effect. Both laser beams (10.49 and 9.0 eV) were kept at the same intensity of $2 \pm 1 \times 10^{10}$ photons per pulse. Above the substrate, the laser beam has a diameter of $2.0 \pm 0.2 \text{ mm}$ and passes the substrate at a distance of $2.0 \pm 0.4 \text{ mm}$. This means that subliming molecules are ionized in a region about two to four millimeters above the substrate. After ionization, they were detected using a reflectron time-of-flight mass spectrometer (ReTOF; Jordan TOF Products, Inc.). The flight time to mass-to-charge conversion was carried out by

Table 1
Structures, Masses, Names, and Calculated Ionization Energies of the Species Under Discussion

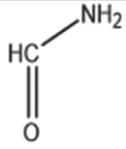
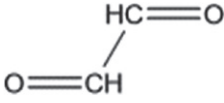
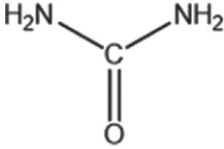
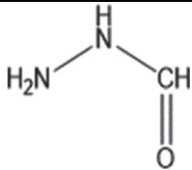
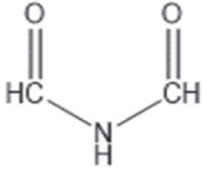
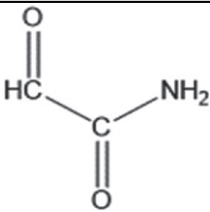
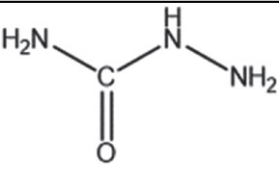
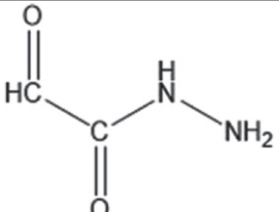
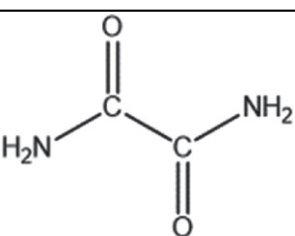
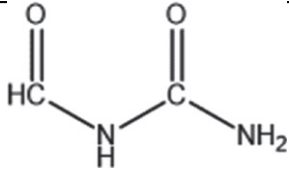
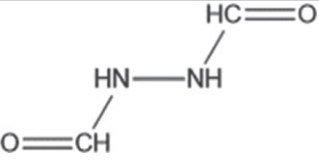
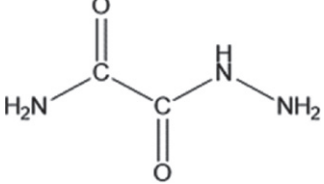
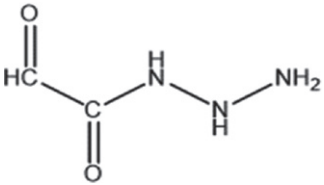
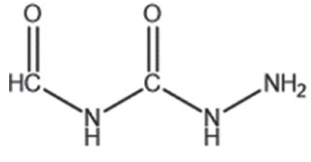
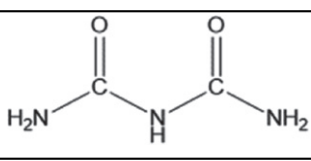
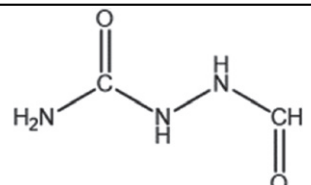
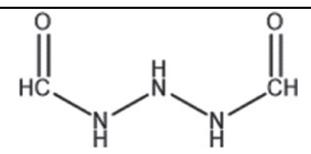
Structure	Mass	Formula	Name	Ionization Energy (eV)	
				Experimental	Calculated
$\text{H}_2\text{C}\equiv\text{O}$	30	H_2CO	formaldehyde	10.88	10.9
	45	HCONH_2	formamide	10.15	10.24
	58	$\text{C}_2\text{O}_2\text{H}_2$	glyoxal(I, II)	10.2	10.14 (I) 10.16 (II)
	60	$\text{CO}(\text{NH}_2)_2$	urea	9.7	9.87
	60	HCON_2H_3	formic acid hydrazide (I–III)	...	8.66 (I) 8.79 (II) 8.43 (III)
	73	$\text{C}_2\text{O}_2\text{NH}_3$	N-formylformamide	...	9.82
	73	$\text{C}_2\text{O}_2\text{NH}_3$	2-oxoacetamide	...	9.92
	75	CON_3H_5	hydrazine carboxamide	...	8.17
	88	$\text{C}_2\text{O}_2\text{N}_2\text{H}_3$	2-oxoacetohydrazide	...	8.54
	88	$\text{C}_2\text{O}_2\text{N}_2\text{H}_4$	ethanediamide (I–III)	9.41	9.61 (I), 10.24 (II) 10.24 (III)

Table 1
(Continued)

Structure	Mass	Formula	Name	Ionization Energy (eV)	
				Experimental	Calculated
	88	C ₂ O ₂ N ₂ H ₄	formylurea (I–IV)	10.58	9.43 (I), 10.16 (II) 10.39 (III) 10.26 (IV)
	88	C ₂ O ₂ N ₂ H ₄	diformylhydrazine	...	9.36
	103	C ₂ O ₂ N ₃ H ₅	2-hydrazinyl-2-oxoacetamide	...	8.33
	103	C ₂ O ₂ N ₃ H ₅	2-oxo-2-triazylacetaldehyde (I–IV)	...	8.33 (I), 8.48 (II) 8.82 (III) 8.27 (IV)
	103	C ₂ O ₂ N ₃ H ₅	N-formylhydrazinecarboxamide (I to VII)	...	8.24 (I) 8.41 (II) 8.48 (III) 7.90 (IV) 8.25 (V) 8.88 (VI) 9.02 (VII)
	103	C ₂ O ₂ N ₃ H ₅	allophanamide/biuret/2-Imidodicarbonic diamide	...	10.02
	103	C ₂ O ₂ N ₃ H ₅	2-formylhydrazinecarboxamide	...	10.38
	103	C ₂ O ₂ N ₃ H ₅	triazane-1, 3-dicarbaldehyde(I–III)	...	8.97 (I) 8.87 (II) 8.54 (III)

Note. Roman numbers indicate different stereoisomers of the molecule. A detailed listing of all calculated energies, atomic distances, and bond angles is given in the supplementary material (Tables 3 and 4).

exploiting the calibrated time-of-flight data points of molecules with known masses. In a third control experiment (blank), we repeated the 10.49 eV experiment but without exposing the ice to ionizing radiation. We also monitored the

subliming molecules with a conventional residual quadrupole mass spectrometer (Extrel, MAX5001. 2APP3/4P6) operated with an electron current of 2 mA and an ionization energy of 70 eV.

Table 2
Values Used to Determine the Irradiation Dose Per Molecule

Initial kinetic energy of the electrons, E_{init}	5 keV
Irradiation current, I	15 ± 2 nA
Total number of electrons	$(3.4 \pm 0.3) \times 10^{14}$
Average kinetic energy of backscattered electrons, E_{bs}^*	1.1 ± 0.4 keV
Fraction of backscattered electrons, f_{bs}^*	0.3 ± 0.1
Average kinetic energy of transmitted electrons, E_{trans}^*	0.03 ± 0.01 keV
Fraction of transmitted electrons, f_{trans}^*	0.03 ± 0.01
Average penetration depth, l^*	270 ± 80 nm
Density of the ice, ρ	0.95 ± 0.1 g cm $^{-3}$

2.2. Theory

In an attempt to discriminate the structural isomers of (some of) the newly formed molecules, it is crucial to know their ionization energies. Because experimental ionization energies of the majority of the species of interest are rare, the adiabatic ionization energies had to be computed (Tables 1; 3–5). The obtained frequencies were compared to data available from the NIST database (formaldehyde, formamide, glyoxal I, and urea) and we propose three scaling factors for three different regions as follows: 1.00 ± 0.05 for the 400–1000 cm $^{-1}$ region, 0.98 ± 0.01 for the 1001–2500 cm $^{-1}$, and 0.965 ± 0.005 for the 2501–4000 cm $^{-1}$ region (compare also to Table 5). The optimized geometries and harmonic frequencies of the molecules (and its cations) are predicted by the hybrid density functional B3LYP (Lee et al. 1988; Becke 1992a, 1992b, 1993) level of theory with the cc-pVTZ basis set. The energies of these species were refined employing the CCSD(T)/cc-pVTZ with B3LYP/cc-pVTZ zero-point energy corrections (Purvis & Bartlett 1982; Hampel et al. 1992; Knowles et al. 1993; Deegan & Knowles 1994). The energies extrapolated to complete basis set CCSD(T)/CBS limit were obtained from (Zhu & Lin 2009). The GAUSSIAN09 program (Frisch et al. 2009) was utilized via the electronic structure calculations. The adiabatic ionization energies were then calculated by taking the energy difference between the ionic and the lowest lying neutral state calculated at the CCSD(T)/cc-pVTZ with a B3LYP/cc-pVTZ zero-point energy correction level of theory. Previous computations at this level compared with experimentally derived ionization energies suggests that the ionization energies derived from the CCSD(T)/cc-pVTZ with B3LYP/cc-pVTZ zero-point energy correction method are accurate within 0.1–0.2 eV (Kostko et al. 2010; Kaiser et al. 2012).

3. RESULTS

3.1. Infrared Data

A detailed description of the reaction products and intermediates synthesized in irradiated ammonia (NH $_3$)–carbon monoxide (CO) ices was recently made by Jones et al. (2011). Our experiments confirmed those results, and a short summary should suffice here. The main products observed after the irradiation of the ice are the ammonium cation (NH $_4^+$) identified via the ν_4 mode at 1505 cm $^{-1}$ (Hagen 1982), the isocyanate ion (OCN $^-$) via its ν_3 fundamental at 2150 cm $^{-1}$ (Grim et al. 1989; Demyk et al. 1998; Hudson & Moore 2000a; van Broekhuizen et al. 2004; Jones et al. 2011), the formyl radical (HCO) through its ν_3 fundamental at 1851 cm $^{-1}$, formaldehyde (H $_2$ CO) via its ν_2 and ν_3 fundamentals at 1740 and 1510 cm $^{-1}$, and formamide (HCONH $_2$) via its carbonyl stretch (ν_4) at 1695 cm $^{-1}$ (Grim et al. 1989; Brucato et al. 2006;

Bennett et al. 2005; Jones et al. 2011). Three broad absorption features (I–III) could not be assigned to individual molecules, only a variety of *group frequencies* of functional groups. A broad band in the region between 3400 and 3100 cm $^{-1}$ can be attributed to –NH– bending modes of amines as well as N–H and O–H stretches of amines (feature I, Figure 2). The absorption in the region from 1180 to 1040 cm $^{-1}$ could stem from the ν_5 rocking of the –NH $_2$ moiety of urea (CO(NH $_2$) $_2$; Stewart 1957), but also from generic –NH $_2$ and –NH– rocking modes of amines and imides, as well as C–N and C–O stretches (feature II, Figure 2). Third, the broad feature in the region between 1600 and 1740 cm $^{-1}$ can be assigned to molecules carrying the carbonyl functional group (feature III, Figure 2). The featureless infrared absorptions I–III are still observable after heating the substrate to 300 K. The temperature-dependent intensity of the three feature is visualized in Figure 2. Feature I dominated the absorptions; the intensity of feature II at 300 K is approximately 20% of the initial absorption measured at 5 K. Finally, the intensity of feature III decreases almost constantly after about 200 K, and reaches almost background levels at 300 K.

3.2. PI-ReTOF-MS Data

The PI-ReTOF-MS data of the subliming molecules taken at 10.49 and 9.0 eV are compiled in Figure 3. For the 10.49 eV experiment, mass-to-charge ratios up to $m/z = 103$ were detected. These data are dominated by ammonia (NH $_3$; IE = 9.9 eV, $m/z = 17$) subliming in the temperature range from 100 to 110 K. This signal decreases strongly after 110 K, but some intensity remains and is observed up to 300 K, most likely because ammonia is trapped within a matrix of less volatile reaction products and outgasses slowly upon heating the substrate. The second largest ion peak is observed at a mass-to-charge ratio of $m/z = 32$ and is attributable to hydrazine (N $_2$ H $_4$, IE = 8.1 eV, $m/z = 32$). This trace has an onset temperature of 170 K and peaks at 210 K, to decrease down to almost zero intensity at 300 K. The assignment is based on comparisons with earlier results obtained on electron irradiated ammonia (NH $_3$) ices (Zheng et al. 2008; Förstel et al. 2015b). Despite its low ionization energy, almost no hydrazine signal is detected in the 9.0 eV experiment, because the ionization cross-section of hydrazine at 9.0 eV is a factor of more than 100 lower than at 10.49 eV (Syage et al. 1992). The integrated mass spectra along with the TPD profiles of those species subliming beyond 150 K are compiled in Figures 4 and 5, respectively. Starting with mass-to-charge ratio of $m/z = 45$, we observe multiple masses via $m/z = 60$ and $m/z = 75$, up to $m/z = 90$ in *constant* increments of $m/z = 15$ (NH; Figure 4). A second group, also with *constant* mass-to-charge ratio increments of $m/z = 15$ (NH), starts with $m/z = 58$ and includes $m/z = 73$, $m/z = 88$, and $m/z = 103$ (Figure 4).

Let us take a detailed look at the TPD profiles of the masses pertaining to these two groups. The profiles were obtained by integrating along the m/z axis within ± 0.2 u around the respective m/z ratio, and plotting the graphs versus the temperature (Figure 5). Also included in Figure 5 is the trace of a mass-to-charge ratio of $m/z = 30$, as measured using the PI-ReTOF-MS and, as a dotted line, using a conventional mass spectrometer. The TPD profiles from group one ($m/z = 30, 45, 60, 75, 90$) depict an increase in sublimation temperature from about 160 to 250 K, with each –NH– group increasing the sublimation temperature by 20–25 K. The signal at $m/z = 90$ is

Table 3
Calculated Minimum Energy Structures and Energies of the Molecules Under Discussion

	Mass	B3LYP/cc-pVTZ + E_{zpc}^a	E_{zpc}^b	CCSD(T)/cc-pVTZ	CCSD(T)/CBS	IP(eV) ^c	IP(eV) ^d
formaldehyde	30	-114.522889	0.026519	-114.333703	-114.388705	0.00	0.00
formaldehyde ⁺	30	-114.128052	0.023853	-113.937072	-113.985349	10.72	10.90
formamide	45	-169.920272	0.045253	-169.641606	-169.725850	0.0	0.0
formamide ⁺	45	-169.552021	0.045165	-169.274443	-169.349411	9.99	10.24
glyoxal I	58	-227.872923	0.036854	-227.487208	-227.595097	0.0	0.0
glyoxal I ⁺	58	-227.509441	0.033848	-227.118060	-227.219338	9.96	10.14
glyoxal II	58	-227.865951	0.036500	-227.479951	-227.587689	0.0	0.0
glyoxal II ⁺ e	58	-227.032861	0.038018	-227.114265	-227.215685	9.99	10.16
urea	60	-225.300314	0.063620	-224.936903	-225.009721	0.0	0.0
urea ⁺	60	-224.952719	0.061972	-224.581835	-224.685181	9.62	9.87
formic acid hydrazide I	60	-225.241959	0.062772	-224.876770	-224.988178	0.0	0.0
formic acid hydrazide I ⁺	60	-224.930734	0.062046	-224.565091	-224.669116	8.46	8.66
formic acid hydrazide II	60	-225.239234	0.062963	-224.873421	-224.984653	0.0	0.0
formic acid hydrazide II ⁺	60	-224.923914	0.061296	-224.556264	-224.659963	8.58	8.79
formic acid hydrazide III	60	-225.234000	0.062569	-224.867840	-224.979508	0.0	0.0
formic acid hydrazide III ⁺	60	-224.930734	0.062046	-224.565091	-224.669116	8.22	8.43
N-formylformamide	73	-283.271193	0.055440	-282.795845	-282.931781	0.0	0.0
N-formylformamide ⁺	73	-282.922678	0.055478	-282.442280	-282.571016	9.62	9.82
2-oxoacetamide	73	-283.271654	0.055167	-282.797493	-282.934425	0.0	0.0
2-oxoacetamide ⁺	73	-282.921116	0.053295	-282.439112	-282.567974	9.70	9.92
hydrazine carboxamide	75	-280.620608	0.080087	-280.169318	-280.309451	0.0	0.0
hydrazine carboxamide ⁺	75	-280.330903	0.078866	-279.875427	-280.008154	7.96	8.17
ethanediamide I	88	-338.672024	0.073475	-338.109866	-338.275846	0.0	0.0
ethanediamide I ⁺	88	-338.335269	0.072412	-337.764704	-337.921750	9.36	9.61
ethanediamide II	88	-338.654544	0.072889	-338.0927604	-338.2582717	0.0	0.0
ethanediamide II ⁺	88	-338.296296	0.072791	-337.7252288	-337.8819877	10.00	10.24
ethanediamide III	88	-338.654547	0.072886	-338.092758	-338.2582707	0.0	0.0
ethanediamide III ⁺	88	-338.296296	0.072791	-337.7252288	-337.8819877	10.00	10.24
formylurea I	88	-338.653737	0.072945	-338.091709	-338.256524	0.0	0.0
formylurea I ⁺	88	-338.323313	0.073288	-337.753476	-337.910421	9.21	9.43
formylurea II	88	-338.665103	0.073086	-338.102609	-338.267817	0.0	0.0
formylurea II ⁺	88	-338.313055	0.070973	-337.736142	-337.892507	9.91	10.16
formylurea III	88	-338.663037	0.073308	-338.100521	-338.265600	0.0	0.0
formylurea III ⁺	88	-338.300624	0.071119	-337.726212	-337.881752	10.13	10.39
formylurea IV	88	-338.671277	0.073761	-338.109137	-338.274360	0.0	0.0
formylurea IV ⁺	88	-338.306588	0.070937	-337.739028	-337.894447	9.99	10.26
diformylhydrazine	88	-338.608207	0.072100	-338.041764	-338.205870	0.0	0.0
diformylhydrazine ⁺	88	-338.270495	0.070522	-337.704468	-337.860283	9.14	9.36
2-oxoacetylhydrazide	88	-338.581043	0.071944	-338.018778	-338.183052	0.0	0.0
2-oxoacetylhydrazide ⁺	88	-338.275410	0.071293	-337.712570	-337.868685	8.31	8.54
2-formylhydrazinecarboxamide	103	-393.915938	0.086442	-393.270645	-393.458889	0.0	0.0
2-formylhydrazinecarboxamide ⁺	103	-393.559608	0.083283	-392.895369	-393.074222	10.13	10.38
allophanamide	103	-393.976131	0.086775	-393.332741	-393.521345	0.0	0.0
allophanamide ⁺	103	-393.631963	0.083837	-392.968505	-393.150149	9.83	10.02
N-formylhydrazinecarboxamide I	103	-393.966714	0.089709	-393.317080	-393.509235	0.0	0.0
N-formylhydrazinecarboxamide I ⁺	103	-393.672392	0.088141	-393.020280	-393.204958	8.03	8.24
N-formylhydrazinecarboxamide II	103	-393.978029	0.089822	-393.327617	-393.520221	0.0	0.0
N-formylhydrazinecarboxamide II ⁺	103	-393.677583	0.088434	-393.025189	-393.209905	8.19	8.41
N-formylhydrazinecarboxamide III	103	-393.975309	0.090166	-393.325457	-393.517670	0.0	0.0
N-formylhydrazinecarboxamide III ⁺	103	-393.672310	0.088494	-393.019582	-393.204271	8.28	8.48
N-formylhydrazinecarboxamide IV	103	-393.984457	0.090812	-393.335160	-393.527519	0.0	0.0
N-formylhydrazinecarboxamide IV ⁺	103	-393.694356	0.089546	-393.043206	-393.235901	7.91	7.90
N-formylhydrazinecarboxamide V	103	-393.976366	0.090650	-393.327518	-393.519874	0.0	0.0
N-formylhydrazinecarboxamide V ⁺	103	-393.684039	0.089476	-393.031523	-393.215419	8.02	8.25
N-formylhydrazinecarboxamide VI	103	-393.978008	0.090407	-393.328311	-393.520113	0.0	0.0
N-formylhydrazinecarboxamide VI ⁺	103	-393.659884	0.088188	-393.007690	-393.191627	8.66	8.88
N-formylhydrazinecarboxamide VII	103	-393.988495	0.090535	-393.338604	-393.530690	0.0	0.0
N-formylhydrazinecarboxamide VII ⁺	103	-393.665326	0.088358	-393.012654	-393.196853	8.81	9.02
2-oxo-2-triazylacetaldehyde I	103	-393.916520	0.089493	-393.269040	-393.460329	0.0	0.0
2-oxo-2-triazylacetaldehyde I ⁺	103	-393.621987	0.088460	-392.968826	-393.152991	8.14	8.33
2-oxo-2-triazylacetaldehyde II	103	-393.908407	0.088980	-393.260282	-393.451704	0.0	0.0
2-oxo-2-triazylacetaldehyde II ⁺	103	-393.608668	0.087666	-392.954814	-393.138727	8.28	8.48
2-oxo-2-triazylacetaldehyde III	103	-393.904367	0.088629	-393.255220	-393.446661	0.0	0.0
2-oxo-2-triazylacetaldehyde III ⁺	103	-393.594529	0.086909	-392.937728	-393.120882	8.59	8.82

Table 3
(Continued)

	Mass	B3LYP/cc-pVTZ + E_{zpc}^a	E_{zpc}^b	CCSD(T)/cc-pVTZ	CCSD(T)/CBS	IP(eV) ^c	IP(eV) ^d
2-oxo-2-triazylacetaldehyde IV	103	-393.909695	0.089560	-393.262409	-393.453355	0.0	0.0
2-oxo-2-triazylacetaldehyde IV ⁺	103	-393.618624	0.088230	-392.964451	-393.148003	8.07	8.27
triazane-1,3-dicarbalddehyde I	103	-393.930110	0.088835	-393.275606	-393.467226	0.0	0.0
triazane-1,3-dicarbalddehyde I ⁺	103	-393.610910	0.086320	-392.950993	-393.135008	8.76	8.97
triazane-1,3-dicarbalddehyde II	103	-393.935796	0.089491	-393.283602	-393.475145	0.0	0.0
triazane-1,3-dicarbalddehyde II ⁺	103	-393.620200	0.087894	-392.963788	-393.147734	8.66	8.87
triazane-1,3-dicarbalddehyde III	103	-393.932966	0.089492	-393.281500	-393.472917	0.0	0.0
triazane-1,3-dicarbalddehyde III ⁺	103	-393.628750	0.087714	-392.972988	-393.157392	8.35	8.54
2-hydrazinyl-2-oxoacetamide	103	-393.986468	0.090507	-393.337190	-393.530395	0.0	0.0
2-hydrazinyl-2-oxoacetamide ⁺	103	-393.689594	0.089326	-393.037658	-393.223106	8.12	8.33

Notes.^a B3LYP/cc-pVTZ energy with zero-point energy correction in hartree.^b Zero-point energy by B3LYP/cc-pVTZ in hartree.^c Relative ionization potential by CCSD(T)/cc-pVTZ with B3LYP/cc-pVTZ zero-point energy correction in eV.^d Relative ionization potential by CCSD(T)/CBS with B3LYP/cc-pVTZ zero-point energy correction in eV.^e Geometry optimization by MP2/cc-pVTZ.**Table 4**
Geometries Underlying the Calculated Energies Shown in Table 3

Atom	X	Y	Z	Atom	X	Y	Z
formaldehyde				formaldehyde ⁺¹			
C	0.000000	0.000000	-0.525948	C	0.000000	0.000000	-0.523546
O	0.000000	0.000000	0.673146	O	0.000000	0.000000	0.664253
H	0.000000	0.937237	-1.114739	H	0.000000	0.966714	-1.086375
H	0.000000	-0.937237	-1.114739	H	0.000000	-0.966714	-1.086375

(This table is available in its entirety in machine-readable form.)

Table 5
Calculated Infrared Band Positions and Intensities
of the Molecules Under Discussion

formaldehyde			formaldehyde ⁺		
Normal Modes	Frequency (cm ⁻¹)	IR Inten	Normal Modes	Frequency (cm ⁻¹)	IR Inten
ν_1	1202.8816	3.2307	ν_1	842.5894	0.0051
ν_2	1268.3618	12.7933	ν_2	1069.4809	31.4812
ν_3	1536.4668	9.9198	ν_3	1247.8429	111.5985
ν_4	1823.8508	106.9075	ν_4	1707.2398	0.0719
ν_5	2877.6004	68.9883	ν_5	2760.4983	178.2550
ν_6	2931.5040	144.6346	ν_6	2842.4801	171.4517

(This table is available in its entirety in machine-readable form.)

weak, but can clearly be discriminated against the background; this feature stems from the small intensity increase at temperatures above 250 K. The first mass ($m/z = 58$) of the second group ($m/z = 58, 73, 88, 103$) shows an increase in intensity at temperatures above approximately 250 K. The total intensity however is too small to determine a maximum of the TPD profile. For the second group with $m/z = 73, 88, \text{ and } 103$, we also observe that the temperature onset of sublimation increases from about 210 to 250 K as the mass-to-charge rises from 73 to 103. However, the difference between the onset of the sublimation temperature of the traces at $m/z = 73$ and 88 is less than 10 K. Also, the TPD profile at $m/z = 103$ holds very low intensity. This means that a definite onset of the sublimation temperature in this group cannot be claimed

without doubt. The spectra measured with 9.0 eV ionization energy depict no intensity; therefore, the ionization energies of the subliming species of the $m/z = 58\text{--}103$ and $m/z = 30\text{--}90$ groups are above 9.0 eV. Note that at 9.0 eV, a very sharp feature arises at around 110 K. This represents an artifact caused by an increase in chamber pressure when the ammonia sublimes.

3.3. Theory

In order to assign possible reaction products and isomers, the ionization energies of 18 structural isomers and 11 conformers were computed. The molecules were selected to have chain structure (branching was not considered), one and two carboxy groups, and an increasing number of amine groups at all possible positions. Among these 29 species, six ionization energies were determined previously in laboratory experiments: formaldehyde, formamide, glyoxal, urea, ethanediamide, and formylurea (Table 1). A comparison of our level of theory with previous experimental data (Kostko et al. 2010; Kaiser et al. 2012) and with the experimental data compiled in Table 1 suggests that the adiabatic ionization energies are accurate within 0.1–0.2 eV. The only exception is the difference in calculated adiabatic and experimentally determined ionization energy of formylurea of 1.1 eV, which is most likely due to a large difference between the adiabatic and vertical ionization energy. In general, this shift is also found to be large in molecules with a terminal $-\text{N}_2\text{H}_3$ moiety because the chain straightens in the ionic species (i.e., a transition of an sp^3 to an sp^2 hybridized nitrogen atom). The computations suggest that if

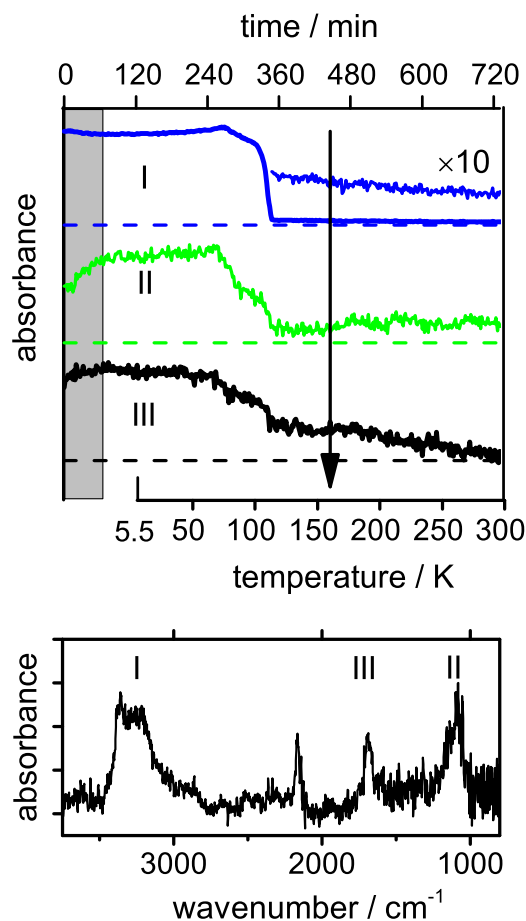


Figure 2. FTIR results. The bottom panel shows the FTIR trace of the irradiated ice at a temperature of 160 K (after carbon monoxide (CO) and ammonia (NH₃) sublimed). Included are the assignments of the broad features described in the text. The top panel shows the temperature dependency of these features. The dashed lines indicate zero intensity. The gray bar indicates the irradiation period and the vertical arrow indicates the temperature from which the sample spectrum in the bottom panel originates.

an -NH- group is inserted into a nitrogen-carbon bond of the CO-NH_2 moiety forming a terminal $\text{-N}_2\text{H}_3$ group, the ionization energy of the molecule strongly decreases by 1.5–1.7 eV. This is evident, for example in case of formamide (HCONH_2 , 10.2 eV) versus formic acid hydrazide (HCON_2H_3 , 8.7 eV) and urea (NH_2CONH_2 , 9.9 eV) versus hydrazine carboxamide ($\text{NH}_2\text{CON}_2\text{H}_3$, 8.2 eV). To a lesser extent, this effect is also observed when an -NHNH- moiety is *formally* formed via insertion of a -NH- into a second -NH- group as, for example, in N-formylformamide (HCO-NH-HCO , 9.8 eV) and diformylhydrazine (HCO-NH-NH-HCO , 9.4 eV). This effect can also explain the difference in the ionization potential of biuret ($\text{NH}_2\text{-CO-NH-CO-NH}_2$, 10 eV) and urazole ($\text{N}_3\text{C}_2\text{O}_2\text{H}_3$, ≤ 9 eV; Ajò et al. 1982). Here, upon ring closure an -N-N- bond forms, thus decreasing the ionization potential by about 1 eV.

4. DISCUSSION

The assignment of the infrared absorptions and of the individual molecules in particular—ammonia (NH_4^+), the isocyanate ion (OCN^-), formyl (HCO), formaldehyde (H_2CO), and formamide (HCONH_2)—was discussed in detail in Section 3.1 and by Jones et al. (2011). In the context of these

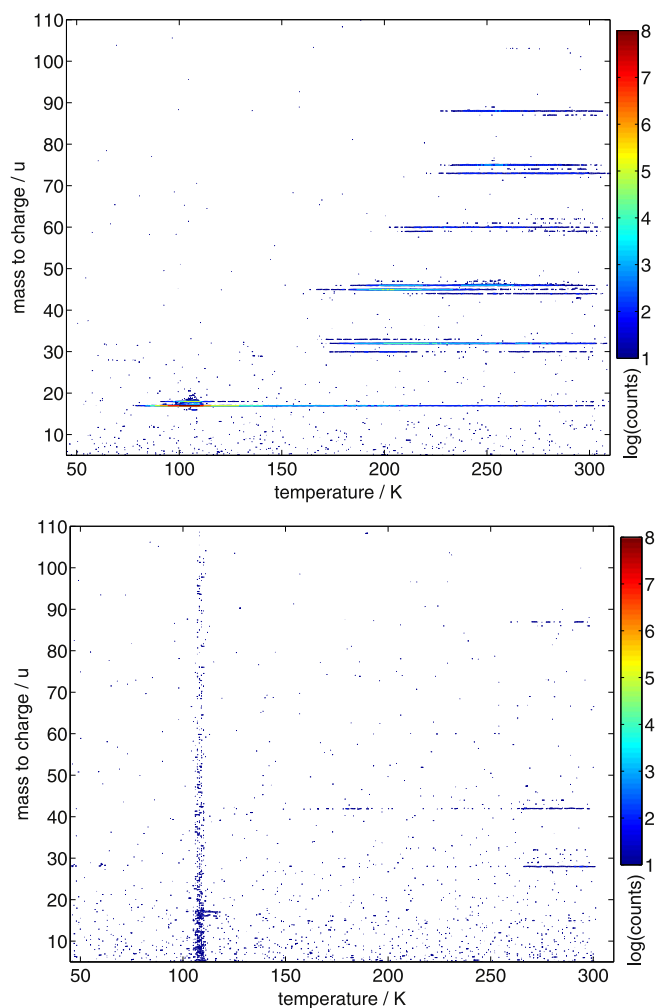


Figure 3. Contour plot of the temperature programmed desorption (TPD) profiles of reactants and products photoionized at 10.49 eV (top) and 9.0 eV (bottom).

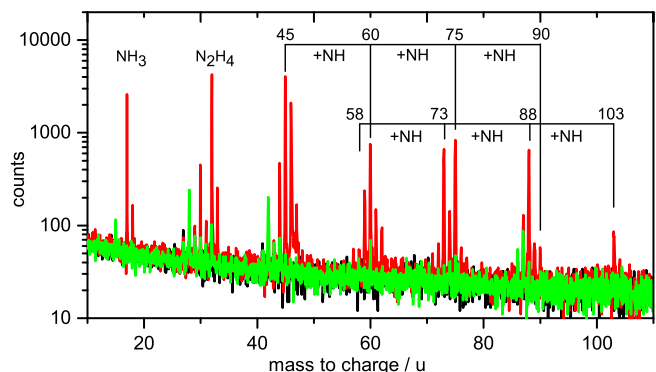


Figure 4. Integrated mass spectra of the subliming molecules in the temperature range from 150 to 300 K measured using 9.0 eV (green) and 10.49 eV (red) photoionization energy. Ion peaks demonstrating the mass growth processes in steps of 15 u are highlighted.

experiments, it is important to stress that the broad absorption features (I–III; Figure 2) are assigned to rocking and bending modes of -NH_2 and -NH- groups, as well as to carbonyl groups (C=O) potentially being adjacent to an -NH- and/or -NH_2 group, which do not decrease to zero intensity upon heating the substrate to 300 K. Up to 20% of the initial intensity

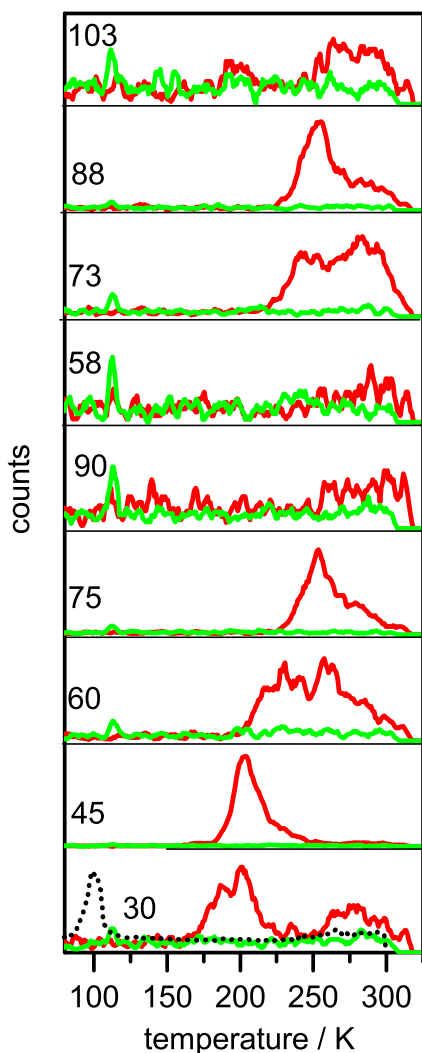


Figure 5. TPD profiles of selected photoionized products demonstrating the mass growth processes by 15 u. The data were recorded exploiting the ReTOF spectrometer at photoionization energies of 10.49 eV (red) and 9.0 eV (green). Solid horizontal lines represent zero for each respective trace. Also shown as a dotted line is the TPD profile at a mass-to-charge ratio of $m/z = 30$, measured with the conventional residual gas analyzer.

remains after the substrate is heated up to room temperature. This demonstrates that a smaller fraction of the residua, which carries the $-\text{NH}_2/-\text{NH}-$ and $\text{C}=\text{O}$ moieties, remains on the substrate, which does not sublime (or sublimates very slowly) at these temperatures.

Let us now concentrate on the interpretation of the PI-ReTOF-MS data (Figures 4 and 5). The main irradiation product at a mass-to-charge ratio of 45 stems from formamide (HCONH_2). It was shown earlier that formamide is a main reaction product in irradiated ammonia (NH_3) carbon monoxide (CO) ices (Milligan & Jacox 1965; Ferris et al. 1974; Hagen 1982; Grim et al. 1989; Demyk et al. 1998; Hudson & Moore 2000b; Jones et al. 2011). An adiabatic ionization energy of about 10 eV cannot be observed with a photoionization energy of 9.0 eV, and subsequently no peak is seen at 45 at the green trace in Figure 4. To our knowledge, this is also the highest mass molecule to be previously observed in the gas phase after $\text{CO}-\text{NH}_3$ ice mixtures were irradiated. At a mass-to-charge ratio of $m/z = 60$ we observe urea. A very small peak at that mass-to-charge ratio is also observed in the 9.0 eV

spectrum (Figure 4). However, the TPD profile measured at 9.0 eV is indistinguishable from the background (Figure 5). With an ionization energy below 9.0 eV (see our calculations in Tables 1 and 3), this peak could stem from the urea isomer formic acid hydrazide (HCONHNH_2) but is too low to allow for an identification. The dotted trace with a mass-to-charge ratio of $m/z = 30$ stems from formaldehyde (H_2CO) and was measured in the same experiment as the 10.49 eV PI-ReTOF-MS spectrum, but using a conventional RGA quadrupole mass spectrometer. Formaldehyde has an ionization energy above 10.49 eV (NIST 2011) and thus cannot be measured in the ReTOF. The peak at a mass-to-charge ratio of $m/z = 30$ shown in Figure 4 thus cannot stem from formaldehyde and is not included in the designated group one in that figure.

An unambiguous identification of the remaining peaks in Figure 4 is not possible using the data available to us. Nevertheless, we can draw more conclusions on the origin of these peaks. The identification of formaldehyde (H_2CO), formamide (HCONH_2), and urea ($\text{CO}(\text{NH}_2)_2$) at mass-to-charge ratios of $m/z = 30, 45,$ and 60 is a strong indication that the increasingly complex peaks observed at 75 and 90 belong to molecules containing one CO group, and three and four $-\text{NH}-$ groups, respectively. This suggests that molecules form with an increasing number of $-\text{NH}-$ groups. Assuming that branching does not take place and by following our assumption that an increasing number of $-\text{NH}-$ groups are added to urea, we can argue that the peak at a mass-to-charge ratio of 75 results from hydrazine carboxamide (CON_3H_5). However, with a calculated vertical ionization energy of 8.2 eV (Tables 1 and 3), it should be observable at the 9.0 eV experiment. The large difference between the adiabatic and vertical ionization energy of hydrazine carboxamide (1.9 eV) is an indication that the ionization cross-section at 9.0 eV may be too low to observe any signal. By adding another $-\text{NH}-$ group, we arrive at a mass-to-charge ratio of 90. Molecules that could pertain to this trace have the chemical formula CON_4H_6 . However, the peak at a mass-to-charge ratio of 90 is very small, and any, more definite structure determinations are impossible. The same trend (adding an $-\text{NH}-$ group) is observable in group two. Starting with a mass-to-charge ratio of 58 we can add up to three $-\text{NH}-$ groups to arrive at a mass-to-charge ratio of 103. It is unclear whether the peak at $m/z = 58$ originates from glyoxal ($\text{C}_2\text{O}_2\text{H}_2$). However, with an ionization energy of 10.2 eV (NIST 2011) it can be observed in the 10.49 eV experiment. The concentration of the formyl radical ($\bullet\text{HCO}$), seems too low to allow for a reaction like $\bullet\text{HCO} + \bullet\text{HCO} (\text{HCO})_2$. Note that we have not observed any IR signal from HCO . It was only reported by Jones et al. (2011) in irradiated ammonia (NH_3) and carbon monoxide (CO) ices that had relative carbon monoxide (CO) to ammonia (NH_3) contents of at least five to two. In addition, the TPD trace of $m/z = 58$ is barely above the noise level and a slight increase is observed at temperatures above 270 K. Nevertheless, assuming that the first molecule in the second group has a mass-to-charge ratio of $m/z = 73$, then we can speculate based on the starting material that they have the chemical formula ($\text{C}_2\text{O}_2\text{NH}_3$, Table 1) are N-formylformamide and 2-oxoacetamide. Both have ionization energies above 9.0 eV and below 10.49 eV, and cannot be discriminated using our data set. A possible parent molecule of the intensity observed at $m/z = 58$ is 2-oxoacetamide. Assuming that these (or one of these) molecules formed, we can now formally insert an $-\text{NH}-$

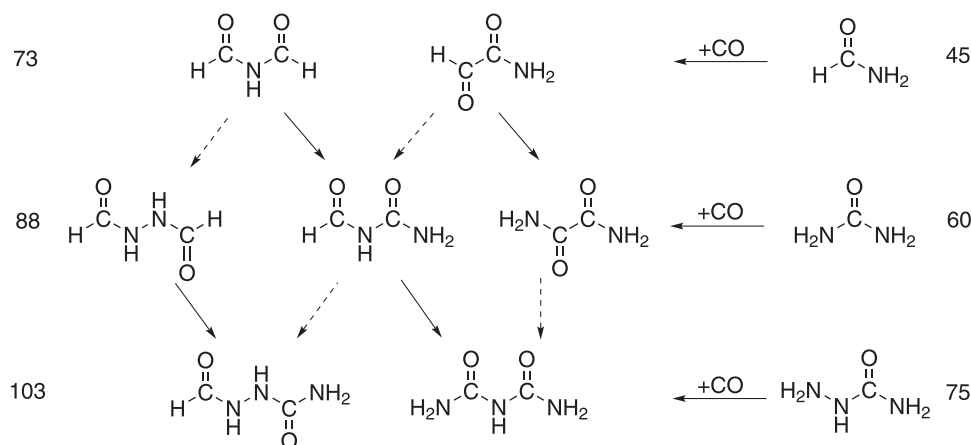


Figure 6. Schematic pathways to the formation of complex molecules, starting with the identified molecules in our experiments from group one in the right side. The arrows mark formal nitrene (NH) insertion or hydrogen loss—amido radical (NH₂) addition. The pathways of sterically less favorable insertion centers are marked with dashed arrows. More favorable cones of acceptances are marked with solid arrows.

group either in between the CO–CO bond of 2-oxoacetamide, in one of the C–H bonds of N-formylformamide or 2-oxoacetamide, or in a C–H bond of either of the two molecules, to end up with the next-higher mass group of possible molecules (Figure 6) with a mass-to-charge ratio of 88. Molecules with this mass-to-charge ratio and with the chemical formula C₂O₂N₂H₄ are 2-oxoacetohydrazide, ethanediamide, formylurea, and diformylhydrazine. Only 2-oxoacetohydrazide has an ionization energy below 9.0 eV and can thus be excluded from the list, because no signal is observed at the 9.0 eV experiment at this mass-to-charge ratio. By adding another –NH– group, we arrive at a mass-to-charge ratio of 103. Here, we already have six possible isomers with the chemical formula C₂O₂N₃H₅, most of which have ionization energies below 9.0 eV. Only biuret and 2-formylhydrazinecarboxamide have ionization energies above 9.0 eV. Biuret is a known and stable molecule and, considering that both formamide and urea are formed in our ices, it is the most likely candidate pertaining to the signal at a mass-to-charge ratio of 103, which is also supported by the scheme shown in Figure 6. The dashed arrows shown in Figure 6 represent geometrically less favorable insertions of nitrene (NH; or additions of NH₂ plus loss of hydrogen) and the solid arrows show more favorable additions. The criteria here is that addition into the C–H bond is sterically more favorable than a central addition. The molecules 2-oxoaceto-hydrazide ($m/z = 88$, C₂O₂N₂H₃), 2-hydrazinyl-2-oxoacetamide, 2-oxo-2-triazylacetaldehyde, triazane-1, 3-dicarbaldehyde, and N-formylhydrazinecarboxamide (all $m/z = 103$, C₂O₂N₃H₅) are omitted in the figure because their ionization energies are below 9.0 eV.

Can some of the observed traces of group one or group two stem from ionic fragments of higher mass molecules? Despite ionizing close to the ionization threshold and thus removing only an outer valence electron, it is known that some molecules can show fragmentation. However, it is usually only a small fraction of parent molecules that fragment upon outer valence ionization close to the ionization threshold, hence the term *soft* ionization. Here we can argue that the traces at mass-to-charge ratios of 30 and 59 above 150 K could show fragments. The trace with a mass-to-charge ratio of 30 shows two distinct peaks (between 170 and 230 K and between 250 and 300 K). The first coincides with the maxima of the traces with mass-to-

charge ratios of 32 and 45. The second with the total intensity of higher mass traces, especially that of the trace with a mass-to-charge ratio of 75. The trace at a mass-to-charge ratio of 59 has a similar temperature profile as the trace with a mass-to-charge ratio of 60. The peak at a mass-to-charge ratio of 59 can therefore be explained by hydrogen loss upon ionization of the species at a mass-to-charge ratio of 60 (Figures 4 and 5).

Where do the remaining peaks in Figure 4 come from? The most intense peak remaining to be discussed is observed at a mass-to-charge ratio of 46. No peak is observed there using 9.0 eV ionization energy. Isotopologues of formamide pertain to about 4% of the observed intensity, but there is no indication that the trace is caused by a fragment of a higher mass molecule. One possibility is that the protonated formamide is observed, which would require the sublimation of a dimer or gas-phase ion-molecule reactions including proton transfer. The peak observed at a mass-to-charge ratio of 87 cannot be explained by hydrogen loss because it is observed at both the 10.49 and 9.0 eV experiment, while the peak at 88 is only observed in the 10.49 eV experiment. It could also be a fragment from a molecule with higher mass, with a fragmentation probability close to 100%. A candidate with a structure similar to those described earlier would be 2-oxopropanamide (C₃H₅NO₂), but its ionization energy lies above 9.0 eV. An assignment of this peak is therefore still under discussion. A comparison of the PI-ReTOF-MS results with the FTIR results adds to the earlier drawn conclusions. The decrease of features I and III (shown in Figure 2) in the temperature range of 150–300 K coincides with the sublimation profiles shown in Figure 5. This shows that the observed decrease in infrared intensity from features I and III is due to the sublimation of molecules carrying the –NH₂ and –NH– moieties.

5. ASTROPHYSICAL IMPLICATIONS

It is well known that the energetic processing of astrophysically relevant ices in laboratories yields complex organics (to name only a few experiments relevant to this study: Milligan & Jacox 1965; Hagen et al. 1979; Agarwal et al. 1985; Bernstein et al. 2002; Chen et al. 2011; Jones et al. 2011; Nuevo et al. 2010; Materese et al. 2014). However, what is clearly new in our study is the observation of the trend to form

complex, amide polymer structures in the energetically processed ices, as well as the online and in situ identification of these complex molecules. Interestingly, a possibly related phenomenon was recently reported to occur on the surface of 67P/Churyumov Gerasimenko (Wright et al. 2015). With their Ptolemy instrument, Wright et al. found indications of the formation of polymers with formaldehyde (H_2CO) as the main building block. It is still under heavy discussion, including the degree of complexity that organic molecules forming in the ISM can reach. The first measurement on the surface of a comet could identify four new complex organics and could have possibly detected more if the sample delivery operated as planned (Goesmann et al. 2015). In the context of our study, we can conclude that molecules with one and two and possibly more amide bonds form easily at very low temperatures in very simple inorganic ices under the influence of energetic particles. We can only detect volatile species in our setup, but knowing that residua are formed and based on the finding that $-\text{NH}-\text{CO}-$ groups form in the ices, we assume that the residua are at least partially made of such amide chain resembling polymers.

Our experiments demonstrate the difficulty of relying on infrared spectra for the identification of individual organic molecules. With an increasing complexity of the formed molecules, the infrared spectra and, in particular, the group frequencies of the products overlap and cannot be distinguished from one another. This is especially the case for molecules that have infrared active functional groups in common. For example, infrared spectra with features similar to those measured here have been assigned to traces of urea in earlier experiments (Grim et al. 1989), where the same ices but different irradiation sources (UV photons) were used. They also claimed derivatized formamide (HCONH_2) as one of the main irradiation products and suggested urea ($\text{CO}(\text{NH}_2)_2$), biuret ($\text{NH}_2\text{CONHCONH}_2$), and oxamide ($\text{NH}_2\text{COCONH}_2$) was formed after analyzing their chemically modified forms with gas chromatography mass/mass spectrometry (GC/MS) studies of the residua. Conclusive assignments based solely on GC/MS studies are difficult, as demonstrated recently by Fang et al. (2015). Knowing that urea homologues form easily in the irradiated ices and that urea desorbs under vacuum conditions at temperatures above 200 K, we can conclude that the infrared features assigned previously to urea are probably caused by a mix of molecules carrying the same functional groups as urea, as evident from the infrared group frequencies compiled (Table 5).

Another important aspect of our study is the prebiotic significance of the detected compounds. Urea, for one, is considered a key prebiotic compound (Horneck & Baumstark-Khan 2012). An endogeneous formation (gas phase as well as liquid phase) of urea is discussed extensively and multiple pathways to form urea exist (Lowe et al. 1963; Lohrmann 1972; Ferris et al. 1974; Hubbard et al. 1975; Sakurai & Yanagawa 1984; Miller 1993; Shapiro 1999). However, a purely endogeneous formation is under debate, due to the seemingly low concentration of cyanates in the oceans of early Earth (Miller 1993) and a limited stability of cyanates at pH values lower than six; at this pH cyanates can hydrolyze to hydrogen cyanide at timescales of geological range (Miller & Orgel 1974). Urea was detected in the Murchison meteorite (Hayatsu et al. 1975) and this indicates that some of the urea on early Earth could have been delivered by meteorites. Also very interesting is the observation of larger, urea related compounds

together with the hydrazine molecule (N_2H_4), because of the possibility to form urazole ($\text{C}_2\text{N}_3\text{O}_2\text{H}_3$) from biuret ($\text{H}_2\text{NCONHCONH}_2$) and hydrazine (N_2H_4) under dry conditions as described by Kolb et al. (1994). The prebiotic relevance of urazole lies in its role in the ribose phosphate backbone formation as discussed by Kolb et al. (1994). We cannot observe urazole or other heterocyclic compounds in our experiment because they do not sublime easily. However, we do observe residua and, considering the products we found, we believe that a search for urazole in these residua should be performed.

Finally, we would like to discuss the selected ice composition. Both, carbon monoxide (CO) and ammonia (NH_3), were detected on ice-coated interstellar grains by the *Spitzer* observatory. Their respective abundances relative to water are typically 20% and 5%, respectively (Pontoppidan et al. 2008; Bottinelli et al. 2010; Reach et al. 2013). Molecular clouds consist of nanometer-sized carbon- and/or silicate-bearing grains with temperatures as low as 10 K. On these grains, icy layers, including carbon monoxide (CO) and ammonia (NH_3) can accrete (Allamandola et al. 1999; Gibb et al. 2004; Boogert et al. 2008). These ices can then be chemically altered through energetic GCR resulting in COM (Greenberg et al. 1983; Greenberg 1984; Sandford & Allamandola 1990; Sandford et al. 1997, 2012; Charnley et al. 2001; Kaiser et al. 2014a). This matter can then enter circumstellar disks in which the formation of planetary bodies and comets takes place, thus also providing the material for meteoritic parent bodies (Ehrenfreund & Charnley 2000). The organic material found on chondrites such as Murchison can be linked to pristine interstellar matter by isotopic studies (Pizzarello & Shock 2010). It is therefore feasible that organics such as those described here can be included into meteoritic parent bodies such as comets (Spencer et al. 2008; Remusat et al. 2010). The compositions of the ices can vary with the temperature of the environment. This was demonstrated for carbon monoxide (CO), whose abundance can vary from 3% to 50% (Chiar et al. 1998; Boogert et al. 2002; Pontoppidan et al. 2003, 2008). The ices selected here present a model ice to understand the formation of COM under anhydrous conditions. The complexity of the found irradiation products justifies this simple model. Only after understanding the processes and products found here can we extend our studies to more complex and realistic systems, such as those incorporating water.

The authors would like to thank the W.M. Keck Foundation and the U.S. National Science Foundation (NSF AST-1505502) for support. M.F. acknowledges funding for a Postdoctoral Fellowship from the Deutsche Forschungsgemeinschaft (FO 941/1). Computer resources at the National Center for High-performance Computer of Taiwan were utilized in the calculations.

REFERENCES

- Adande, G. R., Woolf, N. J., & Ziurys, L. M. 2013, *AsBio*, **13**, 439
 Agarwal, V., Schutte, W., Greenberg, J., et al. 1985, *OLEB*, **16**, 21
 Ajò, D., Casarin, M., Granozzi, G., et al. 1982, *JMoSt*, **82**, 277
 Alexander, C. O. D., Russell, S., Arden, J., et al. 1998, *M&PS*, **33**, 603
 Allamandola, L. J., Bernstein, M. P., Sandford, S. A., & Walker, R. L. 1999, *Evolution of Interstellar Ices* (Berlin: Springer)
 Apene, I., & Mikstais, U. 1978, *Khim-Farm Zh*, **12**, 84
 Baratta, G., & Palumbo, M. 1998, *JOSAA*, **15**, 3076

- Becke, A. D. 1992a, *JChPh*, **96**, 2155
- Becke, A. D. 1992b, *JChPh*, **97**, 9173
- Becke, A. D. 1993, *JChPh*, **98**, 5648
- Bennett, C. J., Jamieson, C., Mebel, A. M., & Kaiser, R. I. 2004, *PCCP*, **6**, 735
- Bennett, C. J., Jamieson, C. S., Osamura, Y., & Kaiser, R. I. 2005, *ApJ*, **624**, 1097
- Bernstein, M. P., Dworkin, J. P., Sandford, S. A., et al. 2002, *Natur*, **416**, 401
- Boogert, A., Blake, G., & Tielens, A. 2002, *ApJ*, **577**, 271
- Boogert, A. C. A., Pontoppidan, K. M., Knez, C., et al. 2008, *ApJ*, **678**, 985
- Bottinelli, S., Boogert, A. C. A., Bouwman, J., et al. 2010, *ApJ*, **718**, 1100
- Brucato, J. R., Baratta, G. A., & Strazzulla, G. 2006, *A&A*, **455**, 395
- Charnley, S. B., Ehrenfreund, P., & Kuan, Y. J. 2001, *AcSpA*, **57**, 685
- Chen, Y. J., Nuevo, M., Chu, C. C., et al. 2011, *AdSpR*, **47**, 1633
- Chen, Y.-J., Nuevo, M., Yih, T.-S., et al. 2008, *MNRASy*, **384**, 605
- Chiar, J., Gerakines, P., Whittet, D., et al. 1998, *ApJ*, **498**, 716
- Costanzo, G., Saladino, R., Crestini, C., et al. 2007, *BMC Evol Biol*, **7**, S1
- Cronin, J., & Chang, S. 1993, *Organic Matter in Meteorites: Molecular and Isotopic Analyses of the Murchison Meteorite*, Vol. 416 (Netherlands: Springer)
- Dederichs, B., Saus, A., & Slebertz, H. 1975, Radiation chemical addition of formamide to alpha -olefins (Inst. Tech. Chem. Petrolchem., Tech. Hochsch. Aachen, Aachen, Fed. Rep. Ger.), <http://www.osti.gov/scitech/biblio/4208412>
- Deegan, M. J. O., & Knowles, P. J. 1994, *CPL*, **227**, 321
- d'Hendecourt, L. B., & Allamandola, L. J. 1986, *A&AS*, **64**, 453
- Demyk, K., Dartois, E., & d'Hendecourt, L. 1998, *A&A*, **339**, 553
- Drouin, D., Couture, A. R., Joly, D., et al. 2007, *Scanning*, **29**, 92
- Ehrenfreund, P. 1999, *Laboratory Astrophysics and Space Research*, Vol. 236 (Berlin: Springer)
- Ehrenfreund, P., & Charnley, S. B. 2000, *ARA&A*, **38**, 427
- Elsila, J. E., Dworkin, J. P., Bernstein, M. P., et al. 2007, *ApJ*, **660**, 911
- Fang, M., Ivanisevic, J., Benton, H. P., et al. 2015, *AnaCh*, **87**, 10935
- Ferris, J. P., Williams, E. A., Nicodem, D. E., et al. 1974, *Natur*, **249**, 437
- Förstel, M., Maksyutenko, P., Jones, B. M., et al. 2015a, *ChCom*, **52**, 721
- Förstel, M., Maksyutenko, P., Jones, B. M., et al. 2015b, *CP*, **15**, 16
- Frisch, M. J., Trucks, G. W., Schlegel, H. B., et al. 2009, *Gaussian 09 Revision E.01* (Wallingford, CT: Gaussian, Inc.)
- Fulvio, D., Sivaraman, B., Baratta, G. A., et al. 2009, *AcSpA*, **72**, 1007
- Gerakines, P. A., Schutte, W. A., Greenberg, J. M., & van Dishoeck, E. F. 1995, *A&A*, **296**, 810
- Gibb, E. L., Whittet, D. C. B., Boogert, A. C. A., & Tielens, A. G. G. M. 2004, *ApJS*, **151**, 35
- Glavin, D. P., Dworkin, J. P., Aubray, A., et al. 2006, *M&PS*, **41**, 889
- Goesmann, F., Rosenbauer, H., Bredehöft, J. H., et al. 2015, *Sci*, **349**, 6247
- Gottlieb, C., Palmer, P., Rickard, L., & Zuckerman, B. 1973, *ApJ*, **182**, 699
- Greenberg, J. M. 1984, *OrLi*, **14**, 25
- Greenberg, J. M., Van de Bult, C. E. P. M., & Allamandola, L. J. 1983, *JPhCh*, **87**, 4243
- Grim, R. J. A., Greenberg, J. M., DeGroot, M. S., et al. 1989, *A&AS*, **78**, 161
- Hagen, W. 1982, PhD thesis, Univ. Leiden
- Hagen, W., Allamandola, L. J., & Greenberg, J. M. 1979, *Ap&SS*, **65**, 215
- Halfen, D., Ilyushin, V., & Ziurys, L. 2011, *ApJ*, **743**, 60
- Hampel, C., Peterson, K. A., & Werner, H.-J. 1992, *CPL*, **190**, 1
- Hayatsu, R., Studier, M. H., Moore, L. P., & Anders, E. 1975, *GeCoA*, **39**, 471
- Hepburn, J. W. 1994, *Laser Techniques in Chemistry* (New York, NY: Wiley)
- Hilbig, R., Hilber, G., Lago, A., et al. 1986, *Proc. SPIE*, **0613**, 48
- Hilbig, R., & Wallenstein, R. 1982, *ApOpt*, **21**, 913
- Hollis, J. M., Lovas, F. J., Remijan, A. J., et al. 2006, *ApJL*, **643**, L25
- Horneck, G., & Baumstark-Khan, C. 2012, in *Astrobiology: The Quest for the Conditions of Life*, ed. G. Horneck, & C. Baumstark-Khan (Dordrecht: Springer Science+Business Media)
- Hubbard, J. S., Voecks, G. E., Hobby, G. L., et al. 1975, *JMolE*, **5**, 223
- Hudgins, D., Sandford, S., Allamandola, L., & Tielens, A. 1993, *ApJS*, **86**, 713
- Hudson, R. L., & Moore, M. H. 2000a, *Icar*, **145**, 661
- Hudson, R. L., & Moore, M. H. 2000b, *A&A*, **357**, 787
- Hudson, R. L., Moore, M. H., Dworkin, J. P., et al. 2008, *AsBio*, **8**, 771
- Johnson, R. E. 1990, *Energetic Charged-Particle Interactions with Atmospheres and Surfaces*, Vol. 19 (New York: Springer)
- Jones, B. M., Bennett, C. J., & Kaiser, R. I. 2011, *ApJ*, **734**, 78
- Jones, B. M., & Kaiser, R. I. 2013, *JPhChL*, **4**, 1965
- Jones, B. M., Kaiser, R. I., & Strazzulla, G. 2014, *ApJ*, **781**, 85
- Kaiser, R. I., Krishtal, S. P., Mebel, A. M., et al. 2012, *ApJ*, **761**, 178
- Kaiser, R. I., Maity, S., & Jones, B. M. 2014a, *Angewandte Chemie*, **54**, 195
- Kaiser, R. I., Maity, S., & Jones, B. M. 2014b, *PCCP*, **16**, 3399
- Kaiser, R. I., Stockton, A. M., Kim, Y. S., et al. 2013, *ApJ*, **765**, 111
- Knowles, P. J., Hampel, C., & Werner, H. J. 1993, *JChPh*, **99**, 5219
- Kolb, V., Dworkin, J., & Miller, S. 1994, *JMolE*, **38**, 549
- Kostakis, I. K., Elomri, A., Seguin, E., et al. 2007, *Tetrahedron Lett*, **48**, 6609
- Kostko, O., Zhou, J., Sun, B. J., et al. 2010, *ApJ*, **717**, 674
- Kvornolden, K., Lawless, J., Pering, K., et al. 1970, *Natur*, **228**, 928
- Lambert, J.-F. 2008, *OLEB*, **38**, 211
- Lambert, J.-F., Stievano, L., Lopes, I., et al. 2009, *P&SS*, **57**, 460
- Lee, C., Yang, W., & Parr, R. G. 1988, *PhRvB*, **37**, 785
- Lohrmann, R. 1972, *JMolE*, **1**, 263
- Lowe, C., Rees, M., & Markham, R. 1963, *Natur*, **199**, 219
- Maity, S., Kaiser, R. I., & Jones, B. M. 2014a, *ApJ*, **789**, 36
- Maity, S., Kaiser, R. I., & Jones, B. M. 2014b, *FaDi*, **168**, 485
- Materese, C. K., Cruikshank, D. P., Sandford, S. A., et al. 2014, *ApJ*, **788**, 111
- Miller, S. L. 1993, *Organic Geochemistry* (Berlin: Springer)
- Miller, S. L., & Orgel, L. E. 1974, *The Origins of Life on the Earth* (Englewood Cliffs, NJ: Prentice-Hall)
- Milligan, D. E., & Jacox, M. E. 1965, *JChPh*, **43**, 4487
- Munoz Caro, G. M., Meierhenrich, U. J., Schutte, W. A., et al. 2002, *Natur*, **416**, 403
- NIST 2011, NIST Chemistry WebBook
- Nuevo, M., Bredehöft, J. H., Meierhenrich, U. J., et al. 2010, *AsBio*, **10**, 245
- Peeters, Z., Botta, O., Charnley, S. B., et al. 2003, *ApJL*, **593**, L129
- Pizzarello, S., & Shock, E. 2010, *Cold Spring Harbor Perspectives in Biology*, **2**, a002105
- Pontoppidan, K. M., Boogert, A. C. A., Fraser, H. J., et al. 2008, *ApJ*, **678**, 1005
- Pontoppidan, K. M., Fraser, H. J., Dartois, E., et al. 2003, *A&A*, **408**, 981
- Purvis, G. D., & Bartlett, R. J. 1982, *JChPh*, **76**, 1910
- Reach, W. T., Kelley, M. S., & Vaubaillon, J. 2013, *Icar*, **226**, 777
- Remijan, A. J., Snyder, L. E., McGuire, B. A., et al. 2014, *ApJ*, **783**, 77
- Remusat, L., Guan, Y., Wang, Y., & Eiler, J. 2010, *ApJ*, **713**, 1048
- Robert, F., & Epstein, S. 1982, *GeCoA*, **46**, 81
- Romanescu, C., Marschall, J., Kim, D., et al. 2010, *Icar*, **205**, 695
- Sakurai, M., & Yanagawa, H. 1984, *OrLi*, **14**, 171
- Saladino, R., Botta, G., Delfino, M., & Di Mauro, E. 2013, *CEJ*, **19**, 16916
- Saladino, R., Crestini, C., Ciciriello, F., et al. 2007, *Chemistry & Biodiversity*, **4**, 694
- Sandford, S. A., Allamandola, L. A., & Bernstein, M. P. 1997, *Astr Soc P*, **122**, 201
- Sandford, S. A., & Allamandola, L. J. 1990, *ApJ*, **355**, 357
- Sandford, S. A., Nuevo, M., & Materese, C. K. 2012, *M&PSA*, **75**, 5071
- Satorre, M. Á., Leliwa-Kopystynski, J., Santonja, C., & Luna, R. 2013, *Icar*, **225**, 703
- Shapiro, R. 1999, *PNAS*, **96**, 4396
- Spencer, M. K., Hammond, M. R., & Zare, R. N. 2008, *PNAS*, **105**, 18096
- Stewart, J. E. 1957, *JChPh*, **26**, 248
- Syage, J. A., Cohen, R. B., & Steadman, J. 1992, *JChPh*, **97**, 6072
- van Broekhuizen, F. A., Keane, J. V., & Schutte, W. A. 2004, *A&A*, **415**, 425
- Westley, M. S., Baratta, G. A., & Baragiola, R. A. 1998, *JChPh*, **108**, 3321
- Wright, I. P., Sheridan, S., Barber, S. J., et al. 2015, *Sci*, **349**, 6427
- Yang, J., & Epstein, S. 1983, *GeCoA*, **47**, 2199
- Zheng, W., Jewitt, D., Osamura, Y., & Kaiser, R. I. 2008, *ApJ*, **674**, 1242
- Zhu, R. S., & Lin, M. C. 2009, *CPL*, **478**, 11